HYDROLOGICAL CONNECTIVITY PATTERNS AND THEIR ECO-HYDROLOGICAL IMPLICATIONS IN THE DASHA RIVER, CHINA

HUANG, Q.* – OUYANG, L. – WANG, Z. M. – LIN, J. Y.

School of Materials and Environmental Engineering, Shenzhen Polytechnic University, Shenzhen 518055, China

**Corresponding author*
e-mail: huangq52@szpu.edu.cn

(Received 5th Mar 2025; accepted 22nd Apr 2025)

Abstract. This study establishes a methodological paradigm for urban river connectivity assessment and provides actionable insights for designing ecologically informed river management strategies in anthropogenically modified watersheds. It also evaluates hydrological connectivity and ecological impacts in urban rivers modified by anthropogenic activities, using the Dasha River in Shenzhen city, southeastern China as a case study. An integrated framework combining graph theory and isotope tracing, supported by weekly eco-hydrological monitoring, revealed spatiotemporal connectivity patterns and ecological responses. The key findings were the followings: (1) Spatial heterogeneity dominated connectivity, with upper-midstream segments (index = 0.88–1.42) exceeding downstream reaches (0.11–0.12), driven by natural hydrology and human modifications. (2) Seasonal connectivity peaked in summer-autumn-winter, but winter artificial water replenishment induced isotopic decoupling, creating a vulnerable "high-connectivity, low-correlation" pseudo-state. (3) Connectivity strongly correlated with runoff regulation (+), minimally influenced soil moisture, enhanced water self-purification, and stabilized water quality. Riparian vegetation responses were distance-dependent: connectivity correlations weakened with lateral distance from the channel. This work establishes a methodological paradigm for urban river connectivity assessment and informs ecologically adaptive management strategies in watersheds affected by anthropogenic activities.
Keywords: *hydroecology, graph theory, stable isotopes, pseudo-connectivity phenomenon, Dasha River*

Introduction

River ecosystems function as pivotal regulators of global biogeochemical cycles, energy cascades, and ecological signaling, forming the foundation for sustainable human development through their contributions to water security, agricultural productivity, climate modulation, and socio-economic services (Best, 2019; Wang et al., 2025; Shi et al., 2025) These ecosystem services fundamentally depend on the structural and functional integrity of hydrological connectivity—a multi-dimensional continuum comprising of: longitudinal (headwater-to-estuary material flux), lateral channel-floodplain reciprocity), vertical (surface-subsurface water interchange), and temporal (hydrological regime synchronization) connectivity (Barcken and Croke, 2007). This interconnected matrix governs critical processes including sediment dynamics, nutrient spiraling, biotic dispersal (Lei et al., 2024; Hu et al., 2024; Wan et al., 2025), while simultaneously shaping geomorphic architectures, habitat mosaics, and ecological succession trajectories.

Since the modern era, intensive anthropogenic pressures have impaired hydrological connectivity in 63% of global river corridors (Grill et al., 2019). Zarfl et al. (2015) established strong correlations between dam construction and river fragmentation, documenting 62% and 54% fragmentation index increases in the Mississippi and

http://www.aloki.hu ● ISSN 1589 1623 (Print) ● ISSN 1785 0037 (Online)
DOI: http://dx.doi.org/10.15666/aeer/2304_71377151

Yangtze River basins, respectively. In China's Yangtze Plain, flood control infrastructure (sluices and levees) has disconnected 130 lakes from the main channel, reducing floodplain wetland coverage from 28.3% in the 1930s to 8.0% in the 2020s (Li et al., 2024). Such connectivity degradation undermines river ecosystem multifunctionality (Cai et al., 2021; Guo et al., 2024; Gao et al., 2024), highlighting the urgent need to decipher connectivity-ecology coupling mechanisms for effective restoration.

Hydrological connectivity assessment has progressed through multiscale methodological innovations. Liu et al. (2025) developed slope-catchment area indices to decode vegetation spatial patterns in the Tarim River Basin. Jiang et al. (2025) employed Euclidean distance metrics to quantify connectivity drivers (elevation gradients, climatic factors, land use changes) in the Dongjiang River Basin. Mu et al. (2024) combined geostatistical connectivity functions with remote sensing to reconstruct 38-year spatiotemporal dynamics in the Wusuli River. Han et al. (2024) applied graph theory to optimize water network connectivity in the Jialu River system. Concurrently, stable hydrogen-oxygen isotope tracers have advanced hydrological connectivity diagnostics (Zhang et al., 2023; Wu et al., 2024; Zheng et al., 2025).

As a representative urban river in Shenzhen, China, the Dasha River demonstrates compounded ecological crises arising from the synergistic pressures of rapid urbanization (Zou et al., 2024; Qiao et al., 2024). Over three decades, 83% of its channel has been artificially hardened, while lateral floodplain inundation frequency decreased sharply from 12 to 2 annual events (Shenzhen Water Authority, 2022). As Nanshan District's primary water source, the river faces competing demands for municipal supply, flood mitigation, and recreational use. Although the municipal Blueway Project achieved 58% NH_3-N concentration reductions (Wang et al., 2020), management fragmentation persists: channel hardening disrupts hyporheic exchange processes (Yang et al., 2023), while reservoir operations override natural flow regimes (Xue et al., 2024; Dang et al., 2025). A connectivity focused framework is critically needed to reconcile hydrological processes with ecological functionality. However, systematic investigations of the Dasha River's hydrological connectivity patterns and their ecological consequences remain absent. This study bridges this knowledge gap through high-resolution eco-hydrological monitoring, connectivity quantification, and mechanistic analysis, providing actionable insights for sustainable river management.

Materials and methods

Study area

The Dasha River (22°33′N, 113°54′E) is a pluvial system in Shenzhen, China, situated within a subtropical monsoon climate zone. Originating from Yangtai Mountain, the river flows 13.7 km through a 90.7 km² catchment before emptying into Shenzhen Bay (*Fig. 1*). The basin exhibits characteristic monsoonal hydrometeorology: elevated thermal regimes (mean annual temperature: 22.4°C) coupled with marked precipitation seasonality (annual total: 1981 mm; 85.3% occurring April-September (Fu et al., 2020), generating distinct seasonal discharge pulses. Two strategic reservoirs—Changlingbei (capacity: 1.2×10^6 m³) and Xili (32.38×10^6 m^3)—serve critical water regulation functions, collectively supplying > 70% of Nanshan District's potable water demand. Intensive urbanization has precipitated extensive fluvial modification, with artificial channelization hardening 83% of the fluvial corridor, leaving < 15% retaining

http://www.aloki.hu ● ISSN 1589 1623 (Print) ● ISSN 1785 0037 (Online)
DOI: http://dx.doi.org/10.15666/aeer/2304_71377151

natural riparian characteristics (Shenzhen Water Authority, 2022). Riparian vegetation comprises a successional mosaic dominated by secondary herbaceous communities (predominantly *Galium aparine* and *Chrysanthemum indicum L.*) interspersed with anthropogenic arboreal plantings (*Cercis chinensis Bunge*, *Cinnamomum camphora*, *Ficus religiosa*).

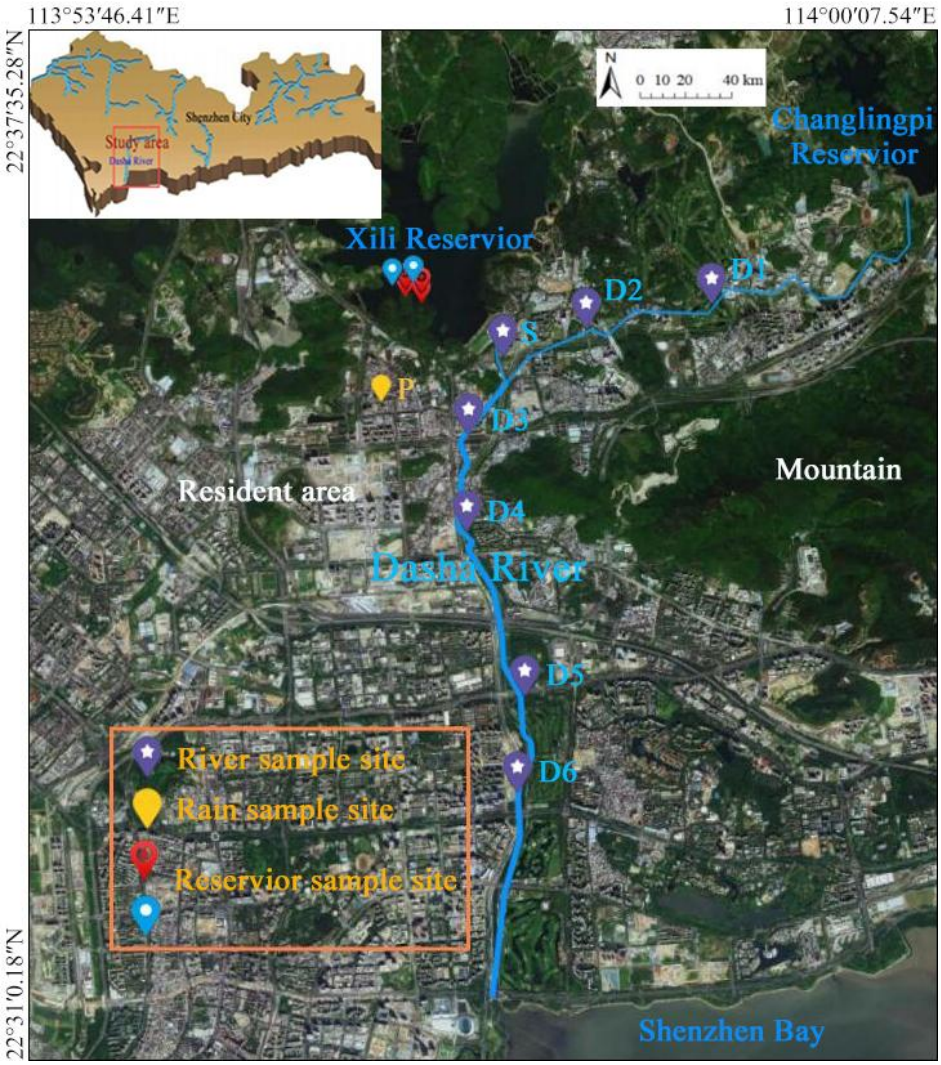

Figure 1. *Schematic map of the study area and sampling points*

Sample collection and processing

This study conducted weekly eco-hydrological monitoring of the Dasha River from November 2023 to October 2024 to establish a multidimensional dataset integrating hydrological and ecological parameters. Six sampling points were established along the longitudinal gradient (*Fig. 1*): D1–D2 (upper reach), D3–D4 (middle reach), and D5–D6 (lower reach). At each point, river water samples were collected, with simultaneous measurements of hydromorphological parameters (width-depth ratio, cross-sectional area) and hydrological-related variables (water level, flow velocity, discharge, and soil moisture). To assess hydrological connectivity impacts on eco-hydrological processes, riparian soil samples (0–50 cm depth) were collected at D2 and D3, while plant xylem

http://www.aloki.hu ● ISSN 1589 1623 (Print) ● ISSN 1785 0037 (Online)
DOI: http://dx.doi.org/10.15666/aeer/2304_71377151

and leaf samples were obtained from D2, D3, and D5. Specific sampling targets were: D2: *Galium aparine* (bankline, 0–1 m), *Chrysanthemum indicum L.* (mid-riparian, 3-m from bank), and *Cercis chinensis Bunge* (terrace margin, 10-m from bank). D3: *Galium aparine* (bankline, 0–1 m), *Chrysanthemum indicum L.* (mid-riparian, 3-m from bank), and *Cinnamomum camphora* (terrace margin, 10-m from bank). D5: *Chrysanthemum indicum L.* (bankline, 0–1 m), and *Ficus religiosa* (terrace margin, 10-m from bank). Additional sampling included reservoir discharge at spillway S and precipitation at point P. All samples were stored in acid-washed polyethylene bottles, sealed, and refrigerated at 4°C until analysis. The dataset comprised 680 valid samples: 300 river water, 50 reservoir discharge, 100 soil, 167 plant xylem, 100 plant leaf, and 63 rainwater samples. Data completeness reached 94%, with missing values on 7 February, 14 February, and 14 August 2024 confirmed as randomly distributed through Kolmogorov-Smirnov testing ($p > 0.05$). Xili Reservoir water samples served for cross-validation.

Water quality analysis: Field measurements of pH (±0.01), electrical conductivity (EC) (±1 μS/cm), and dissolved oxygen (DO) (±0.1 mg/L) employed a HACH HQ40d multiparameter probe (Hach Company, USA). Laboratory determinations of total nitrogen (TN) and total phosphorus (TP) followed persulfate digestion with flow injection analysis (FIA QC8500, LACHAT Instruments, USA), achieving detection limits of 0.02 mg/L and 0.001 mg/L respectively.

Plant physiological monitoring: Leaf reflectance spectra (350–2500 nm) were recorded using an ASD FieldSpec 3 hyperspectral spectrometer (Malvern Panalytical, UK). Total chlorophyll content in leaves collected during the initial three months was quantified through acetone extraction and spectrophotometric analysis using a Shimadzu UV-2600i UV-Vis spectrophotometer (Shimadzu Corp., Japan), establishing a spectral inversion model with calibration curve $R^2 > 0.98$.

Stable isotope analysis: Soil water and xylem water were extracted using a LI-2100 automatic cryogenic vacuum distillation water extraction system (LICA United Tech, Beijing, China). Hydrogen (δ^2H) and oxygen (δ^{18}O) isotopic compositions of all aqueous samples (river, soil, plant, precipitation) were analyzed via LGR-IWA-35EP laser spectroscopy (ABB Ltd., Canada), reported in ‰ relative to VSMOW with precisions of ± 0.1‰ for δ^{18}Oand ± 1‰ for δ^2H (Dansgaard et al., 1964).

$$\delta = \left(\frac{R_{\text{sample}}}{R_{\text{standard}}} - 1 \right) \times 1000\% VSMOW \quad \text{(Eq.1)}$$

where R_{sample} refers to the isotopic ratio of $^{18}O/^{16}O$ or $^{2}H/^{1}H$ in the water samples, while R_{standard} corresponds to the ratio for VSMOW.

Research methods

Hydrological connectivity quantification

This study implemented a graph-theoretic hydraulic connectivity assessment framework (Xu et al., 2012) to quantify the hydrological connectivity dynamics of the Dasha River system. First, a weighted river network graph model was constructed using source/sink points, sampling nodes, and hydraulic structures as topological nodes, with river channels represented as directed edges. The model was formalized as an adjacency matrix ($W = (w_{ij})_{n\times n}$), where w_{ij} denotes the edge weight between adjacent nodes i and j,

http://www.aloki.hu ● ISSN 1589 1623 (Print) ● ISSN 1785 0037 (Online)
DOI: http://dx.doi.org/10.15666/aeer/2304_71377151

and n is the total number of nodes. Next, based on the influence of flow resistance factors (channel length, width, depth, roughness coefficient, and slope) on connectivity, Manning's resistance equation was introduced to couple channel geometric parameters (bottom width, water depth, side slope coefficient) with hydraulic parameters (roughness coefficient, slope). The edge weight was defined as the reciprocal of flow resistance. The edge weight between two adjacent nodes is expressed as:

$$w_{ij} = \frac{1}{H_{ij}} \quad \text{(Eq.2)}$$

where H_{ij} represents the flow resistance between adjacent nodes. According to Manning's formula, H_{ij} can be derived as:

$$v = \frac{1}{k} R^{2/3} S^{1/2} \quad \text{(Eq.3)}$$

$$H = lk \left[\frac{(b + mh)h}{b + 2h\sqrt{1 + m^2}} \right]^{2/3} \quad \text{(Eq.4)}$$

where v is the average flow velocity (m/s), R is the hydraulic radius (m), and l is the flow distance (m). Finally, the maximum edge weight between adjacent nodes was selected to represent the hydraulic conveyance efficiency of the channel segment. The hydrological connectivity degree D_i (dimensionless, 0–1 scale) for any node was calculated as the average of the hydraulic conveyance efficiencies of its upstream and downstream channel segments, while the regional hydrological connectivity D was defined as the mean of all nodal values. A higher D value indicates superior hydraulic continuity, reflecting stronger hydrological connectivity at the node or regional scale.

Isotopic tracing of hydrological connectivity

Hydrogen and oxygen elements in natural water exist as distinct stable isotopes, including ^{1}H, ^{2}H, ^{16}O, ^{17}O, and ^{18}O. Due to mass-dependent differences in physicochemical reaction rates between isotopes, isotopic fractionation occurs during key water cycle processes such as precipitation, evaporation, and runoff. This results in systematic variations in stable isotope abundances or ratios throughout the water cycle, generating characteristic isotopic fingerprints. Consequently, aquatic stable isotopes serve as natural tracers for water cycle studies, enabling qualitative and quantitative investigations of diverse hydrological processes and components. These isotopes have been effectively applied in research areas including atmospheric precipitation moisture sourcing, surface water origin and composition analysis, surface water-groundwater interactions, and groundwater dynamics (Kleine et al., 2021; Alrehaili et al., 2024; Chen et al., 2025). This study analyzed stable hydrogen-oxygen isotope compositions in water samples from upstream, midstream, and downstream reaches of Dasha River. By correlating isotopic signatures with riparian soil and plant xylem water, and integrating the graph-theoretic connectivity metrics, multi-dimensional hydrological connectivity characteristics were elucidated.

http://www.aloki.hu ● ISSN 1589 1623 (Print) ● ISSN 1785 0037 (Online)
DOI: http://dx.doi.org/10.15666/aeer/2304_71377151

Cubist model

A Cubist hybrid regression model was adopted to inversely estimate total leaf chlorophyll content (Chl) from hyperspectral data. Cubist combines rule-based regression trees and piecewise linear models to capture nonlinear relationships, offering high interpretability (Henderson et al., 2005). Two hyperparameters—neighbors (proximity sample count) and committees (ensemble model iterations)—were optimized. Leaf spectral data (400–2400 nm) were partitioned into training and validation sets (3:1 ratio). A Cubist predictive model was trained using measured Chl values from the first three months of leaf samples. Parameter optimization utilized 10-fold cross-validation and grid search for committee numbers (2, 4, 6, 8) and neighbor counts (10, 20, 30, 40). The finalized model predicted Chl for remaining samples based on spectral features.

Results and analysis

Hydrological connectivity characteristics

Longitudinal hydrological connectivity

Based on *Equations 1–3*, the node hydrological connectivity was calculated using hydrological parameters (riverbed width, surface width, water depth, and flow velocity) measured at six river sampling sites. Annual average results are presented in *Table 1*. The connectivity values reveal significant spatial heterogeneity in the longitudinal hydrological connectivity of the Dasha River: Midstream (D3–D4): Highest connectivity (1.39 and 1.67), with faster flow velocities, reflecting enhanced hydraulic efficiency due to channelization and reservoir discharge. Upstream (D1–D2): Moderate connectivity (1.14 and 1.11) and relatively fast flow velocities. Downstream (D5–D6): Connectivity sharply declined to 0.11–0.12, with slow flow velocities, primarily constrained by tidal backwater effects and reclaimed water inputs.

Table 1. *Hydrological parameters and calculated connectivity degrees at Dasha River sampling points*

Sample site	Longitude	Latitude	Riverbed width (m)	Surface width (m)	Water depth (m)	Flow velocity (m/s)	*D* value
D1	113.983	22.594	2.69	4.45	0.22	0.44	0.88
D2	113.957	22.592	3.12	4.98	0.33	0.61	1.03
D3	113.956	22.588	4.38	8.58	0.45	0.59	1.26
D4	113.951	22.573	7.45	11.46	0.30	0.55	1.42
D5	113.955	22.545	29.62	33.82	1.80	0.11	0.12
D6	113.952	22.538	18.44	21.02	2.20	0.15	0.11

Stable hydrogen-oxygen isotope analysis further validated these findings. The δ^2H vs. δ^{18}O plots (*Fig. 2*) deviated markedly from the local meteoric water line (LMWL; (R^2 = 0.59–0.78)), indicating mixed water sources (precipitation, reservoir discharge, reclaimed water, groundwater) and strong evaporation. High δ^{18}O correlations ((r = 0.92) for D1–D2; (r = 0.87) for D3–D4; *Table 2*) confirmed superior longitudinal connectivity in midstream and upstream reaches. Downstream connectivity (D5–D6;

http://www.aloki.hu ● ISSN 1589 1623 (Print) ● ISSN 1785 0037 (Online)
DOI: http://dx.doi.org/10.15666/aeer/2304_71377151

(r = 0.67)) was weakened by external water inputs (e.g., reclaimed water). Isotopic and graph-theoretic results consistently demonstrated a connectivity gradient: midstream > upstream > downstream.

Table 2. *Pearson correlation coefficients (r) for $\delta^{18}O$ values across sampling points*

	D1	D2	D3	D4	D5	D6	S
D1	1.00	0.92	0.47	0.46	0.61	0.48	0.45
D2	0.92	1.00	0.47	0.48	0.66	0.44	0.48
D3	0.47	0.47	1.00	0.87	0.66	0.57	0.71
D4	0.46	0.48	0.87	1.00	0.68	0.61	0.59
D5	0.61	0.66	0.66	0.68	1.00	0.73	0.60
D6	0.48	0.44	0.57	0.61	0.73	1.00	0.37
S	0.45	0.48	0.71	0.59	0.60	0.37	1.00

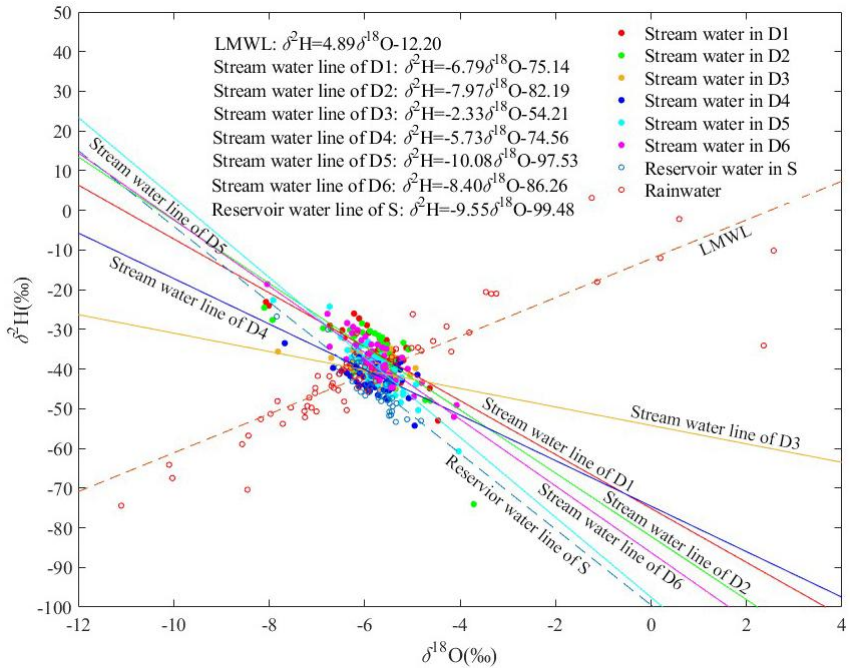

Figure 2. *δ^2H vs. $\delta^{18}O$ scatter plots and regression lines for water samples (D1–D6, S)*

The graph theory-based method for calculating hydrological connectivity cannot discern lateral hydrological connectivity in rivers, whereas stable hydrogen and oxygen isotope analysis in water enables such discrimination. The δ^2H vs. $\delta^{18}O$ relationships for river, soil, and plant xylem water samples at D2, D3, and D5 are shown in *Figure 3*. As seen in *Figure 3a, b*, the δ^2H and $\delta^{18}O$ scatter points of soil water at D2 and D3 clustered along the river water signature, demonstrating that river water is the dominant contributor to riparian soils, with higher lateral hydrological connectivity at these sites. The δ^2H and $\delta^{18}O$ values of plant xylem water at D3 exhibited stronger isotopic affinity to river water than those at D2, particularly for *Galium aparine* (a riparian plant), whose isotopic signatures converged with the river water cluster. This statistical convergence indicates that river water is one of the main water source for riparian vegetation at D3.

http://www.aloki.hu ● ISSN 1589 1623 (Print) ● ISSN 1785 0037 (Online)
DOI: http://dx.doi.org/10.15666/aeer/2304_71377151

The isotopic gradients in plant xylem water further indicate that lateral hydrological connectivity is significantly enhanced at D3 compared to D2. In *Figure 3c*, the δ^2H and δ^{18}O scatter points of plant xylem water at D5 diverged markedly from the river water signature, revealing minimal vegetation dependence on river water and consequently attenuated lateral connectivity at D5. Thus, the lateral hydrological connectivity of the Dasha River follows a distinct spatial hierarchy: midstream > upstream > downstream, with channel hardening identified as the key constraint on lateral connectivity.

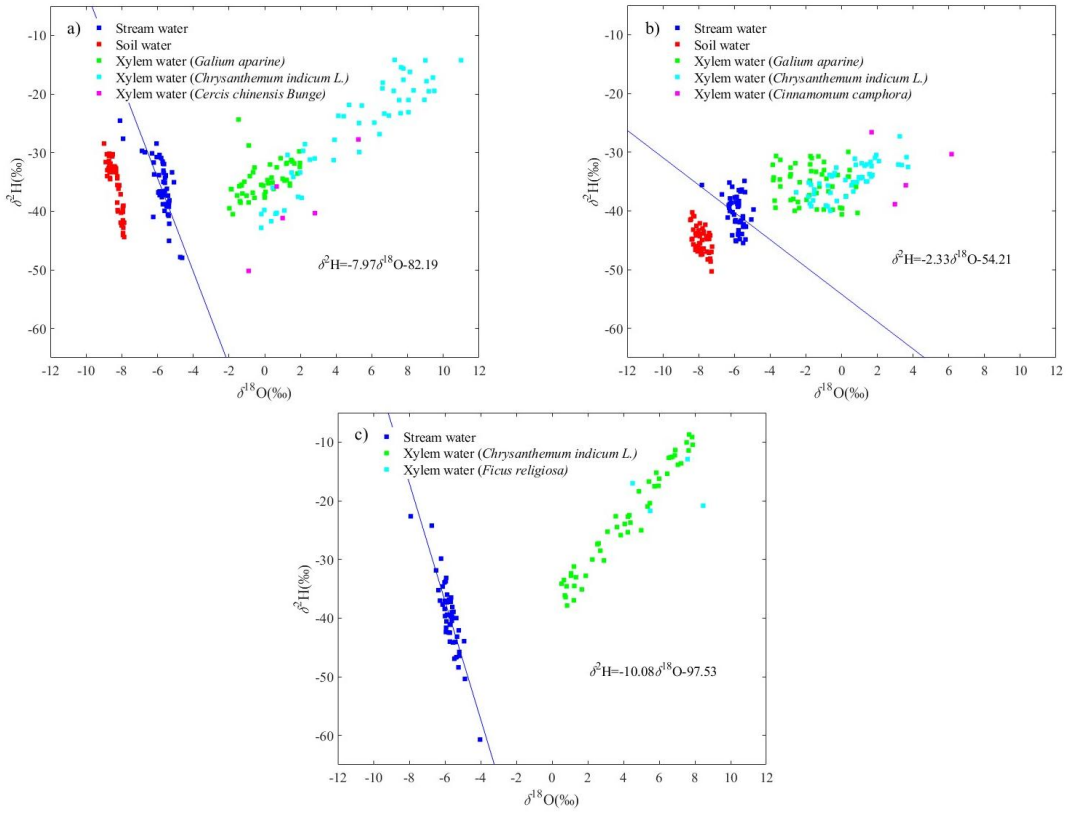

Figure 3. *δ^2H vs. δ^{18}O relationships for river, soil, and xylem water: (a) D2, (b) D3, (c) D5 lateral hydrological connectivity*

Eco-hydrological impacts of hydrological connectivity

Impacts on water quantity

Using the upstream D2 and midstream D3 sites—adjacent areas with relatively strong hydrological connectivity—as representative cases, we selected graph theory-based hydrological connectivity, river discharge, and riparian soil moisture content as indicators to study the impacts of hydrological connectivity on water quantity. During the study period, the average hydrological connectivity at D2 was 1.03 (range: 0.24–1.81), with an average discharge of 0.94 m^3/s (0.09–2.81 m^3/s) and average soil moisture content of 30.23% VWC (21.30–41.70% VWC). At D3, the average hydrological connectivity was 1.26 (0.44–2.06), average discharge was 1.85 m^3/s (0.50–4.46 m^3/s), and average soil moisture content was 31.58% VWC (22.00–37.30% VWC). The Pearson correlation coefficients between hydrological connectivity and discharge or soil moisture content were 0.70 (discharge) and 0.08 (soil moisture) at D2, and 0.85

http://www.aloki.hu ● ISSN 1589 1623 (Print) ● ISSN 1785 0037 (Online)
DOI: http://dx.doi.org/10.15666/aeer/2304_71377151

(discharge) and 0.37 (soil moisture) at D3. Overall, D3, with higher hydrological connectivity, demonstrated superior discharge magnitudes and marginally elevated soil moisture levels, alongside stronger coupling with connectivity metrics, compared to D2. Both D2 and D3 exhibited weak correlations between hydrological connectivity and soil moisture, particularly at D2 (statistically insignificant), consistent with its diminished lateral hydrological connectivity. Thus, hydrological connectivity exerts a more pronounced control on discharge than on soil moisture.

Notably, both D3 and D2 displayed substantial variability in hydrological connectivity and water quantity, indicating system instability. Temporal variations in hydrological connectivity, discharge, and soil moisture content at D2 and D3 during the study period are shown in *Figure 4a*, *b*. As depicted, discharge and hydrological connectivity at both sites followed synchronized temporal trajectories, with peak connectivity corresponding to maximum discharge. Furthermore, D3 exhibited amplified discharge responsiveness to connectivity fluctuations compared to D2. Soil moisture at D3 maintained relatively stable patterns (*Fig. 4b*), whereas D2 showed inverse phase relationships (*Fig. 4a*), attributable to bank irrigation practices and temporal lags in vadose zone water redistribution at D2. Consequently, given D2's compromised lateral hydrological connectivity, hydrological connectivity positively modulates both discharge and soil moisture, though its influence on soil moisture remains highly nonstationary.

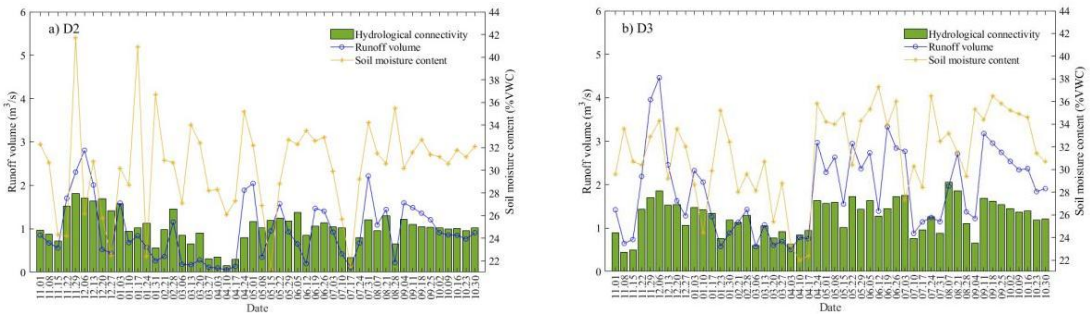

Figure 4. *δ^2H vs. $\delta^{18}O$ scatter plots and regression lines for water samples (D1–D6, S)*

Impacts on water quality

During the study period, the variations in hydrological connectivity and water quality indicators (pH, EC, TDS, DO, TN, TP) at D2 and D3 are shown in *Figure 5* (hydrological connectivity, TN, and TP values were magnified 5× in the figure due to their lower absolute magnitudes relative to other indicators). As seen in *Figures 5* and *6*, TDS and EC exhibited pronounced temporal variability. Hydrological connectivity demonstrated positive associations with TDS at both D2 and D3 (Pearson correlation coefficients: 0.21 and 0.43, respectively) and inverse relationships with EC (−0.20 and −0.53, respectively). Conversely, pH, DO, TN, and TP remained comparatively stable. At D2, hydrological connectivity correlated positively with DO, TN, and TP (0.48, 0.23, and 0.09, respectively) and negatively with pH (−0.28). At D3, hydrological connectivity showed positive correlations with DO and TP (0.15, 0.23) but negative correlations with pH and TN (−0.04, −0.19). Thus, excluding TN, hydrological connectivity at both sites displayed consistent weak-to-moderate linkages with water quality parameters. Notably, D3 (with higher connectivity) generally exhibited stronger

http://www.aloki.hu ● ISSN 1589 1623 (Print) ● ISSN 1785 0037 (Online)
DOI: http://dx.doi.org/10.15666/aeer/2304_71377151

water quality correlations than D2, except for pH and DO. Further analysis of water quality distributions (box plots in *Fig. 7*) revealed a marked prevalence of outliers in water quality indicators at D2 relative to D3 (*Fig. 6a*, *b*), signifying reduced stability in D2's water quality regime. This confirms that elevated hydrological connectivity enhances the self-regulation capacity of aquatic systems, resulting in dampened variability in water quality dynamics.

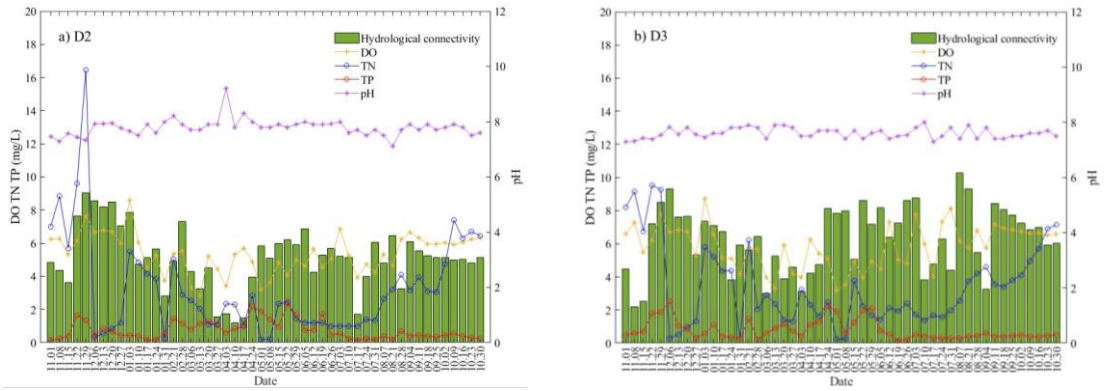

Figure 5. *Temporal variations in connectivity and water quality parameters (DO, TN, TP, and pH) at D2/D3*

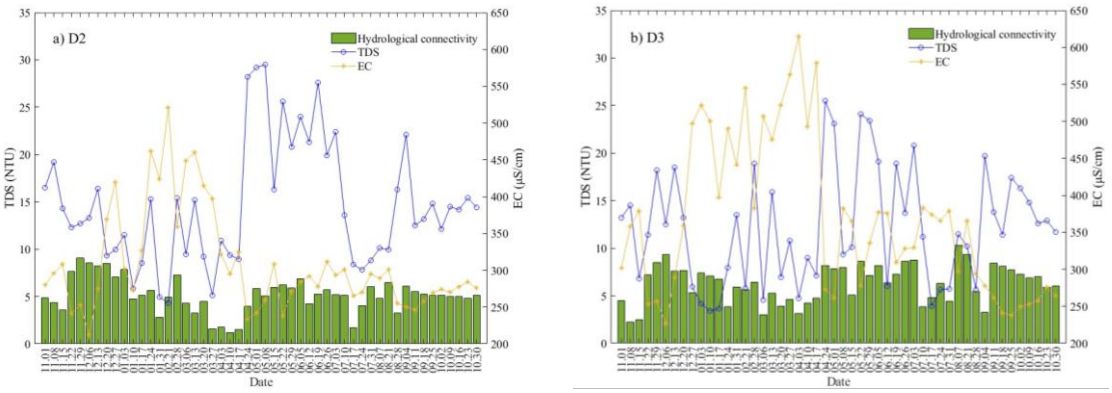

Figure 6. *Temporal variations in connectivity and water quality parameters (TDS and EC) at D2/D3*

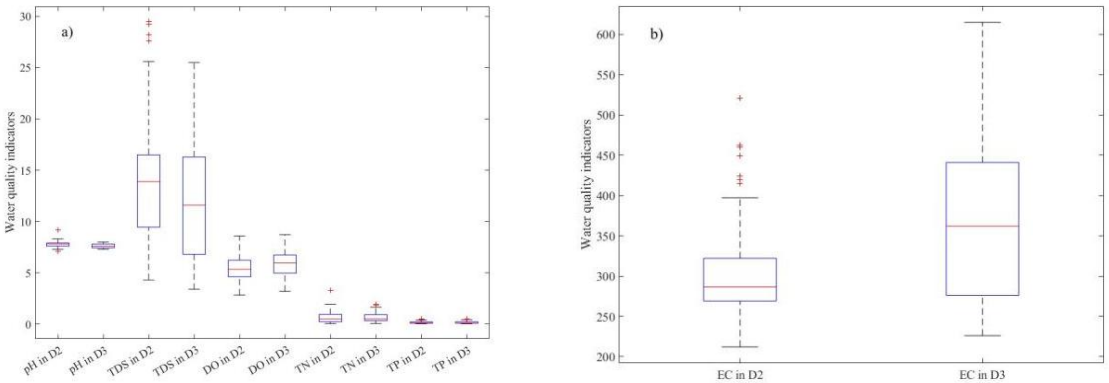

Figure 7. *Boxplots of water quality parameters at D2/D3*

http://www.aloki.hu ● ISSN 1589 1623 (Print) ● ISSN 1785 0037 (Online)
DOI: http://dx.doi.org/10.15666/aeer/2304_71377151

Impacts on plant growth

The constructed Cubist model for plant leaf spectral data and measured total chlorophyll content achieved a prediction root mean square error (RMSEP) of 0.13 mg/g and a bias of -0.01 mg/g. The minimal RMSEP and negligible bias signify high predictive accuracy, confirming the model's robust reliability for estimating total chlorophyll content in plant leaf samples. Temporal dynamics of model-estimated total chlorophyll content and hydrological connectivity at D2 and D3 during the study period are shown in *Figure 8*. Overall, total chlorophyll content displayed negligible correlations with hydrological connectivity, with absolute Pearson correlation coefficients consistently below 0.15. The total chlorophyll content of *Galium aparine* exhibited amplified coupling with hydrological connectivity fluctuations, manifesting locally strengthened correlations during autumn and winter ($r > 0.50$). In contrast, non-riparian species such as *Chrysanthemum indicum L.* and *Cercis chinensis Bunge* (or *Cinnamomum camphora*) showed minimal physiological responsiveness, with weak chlorophyll-hydrological connectivity linkages. Compared to D2, the elevated hydrological connectivity at D3 corresponded to systematically higher total chlorophyll content, reflecting enhanced physiological performance in plants. Notably, the chlorophyll content of *Galium aparine* at D3 demonstrated greater hydrological connectivity-driven variability than at D2.

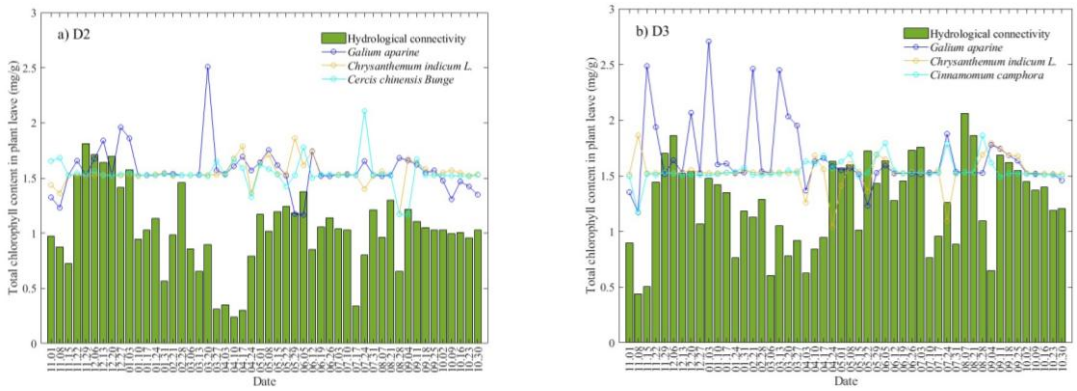

Figure 8. *Temporal variations in connectivity and leaf chlorophyll at D2/D3*

Discussion

This study focuses on the Dasha River, a typical artificially regulated river in southeastern China, revealing significant spatiotemporal heterogeneity characteristics in the hydrological connectivity of urban rivers. The research findings align with those of Xue et al. (2024) and Dang et al. (2025) regarding hydrological heterogeneity in urban rivers. However, through an innovatively constructed "graph theory-isotope tracing" coupled assessment method, we have identified a special hydrological phenomenon of "high connectivity-low correlation" in human-regulated rivers.

Specifically, stable isotope analysis of water bodies (*Table 2*) shows significant correlations in $\delta^{18}O$ values between sections D1-D2, D3-D4, and D5-D6 (summer $r = 0.97$-0.99, autumn $r = 0.81$-0.91, spring/winter $r = 0.64$-0.84), indicating strong longitudinal hydrological connectivity characteristics. However, hydrological connectivity calculations based on graph theory algorithms present a different seasonal pattern: higher connectivity in summer ($D = 0.98$-1.39), autumn ($D = 1.09$-1.47), and winter ($D = 1.29$-1.33), with relatively lower values in spring ($D = 0.79$-1.13).

http://www.aloki.hu ● ISSN 1589 1623 (Print) ● ISSN 1785 0037 (Online)
DOI: http://dx.doi.org/10.15666/aeer/2304_71377151

This seasonal decoupling phenomenon in hydrological connectivity evaluation indicators mainly stems from the interplay of natural hydrological cyclicity and anthropogenic perturbations: during high-flow periods (summer and autumn), high runoff naturally drives synchronous improvement in both hydrological connectivity and isotope correlations; whereas during low-flow periods (winter), although artificial water replenishment (reservoir releases and reclaimed water replenishment) maintains high hydraulic connectivity, significant differences in isotopic composition between different water sources lead to mixed water isotope fingerprints, forming a "high connectivity-low correlation" hydrological homogenization characteristic.

The important finding of this study lies in revealing that while artificial water replenishment measures address water shortages, they simultaneously weaken the ecological indicative function of hydrological connectivity by altering hydrochemical characteristics. However, this study failed to identify the hydrological connectivity threshold for ecological risk generation. Future research could develop hydrological connectivity early-warning models integrating machine learning and isotope tracing to improve the precision management of river water replenishment measures.

Conclusions

Through a one-year high-resolution eco-hydrological monitoring campaign, this study systematically elucidated the spatiotemporal heterogeneity of hydrological connectivity patterns in the Dasha River and their cascading eco-hydrological effects. First, by integrating channel morphology parameters, hydrological metrics, and water isotope data with graph-theoretic topological modeling and stable isotope tracing, we quantified multidimensional hydrological connectivity across distinct river segments. Longitudinally, the Dasha River displayed reach-specific connectivity gradients, with elevated connectivity in upper/mid-reaches and diminished connectivity downstream. Natural drivers (e.g., hydrological pulsatility, tidal backwater effects) and anthropogenic pressures (e.g., channel hardening, reservoir releases, reclaimed water inputs) emerged as dominant control factors. Laterally, connectivity followed similar spatial trends, with upstream/midstream zones exhibiting enhanced river-riparian coupling compared to downstream areas constrained by channel armoring. Temporally, connectivity peaked in summer, autumn, and winter but declined in spring, driven by seasonal runoff dynamics—high wet-season (summer/autumn) discharge amplified connectivity, while anthropogenic winter replenishment sustained hydraulic connectivity but induced isotopic decoupling via mixed-source water blending, creating paradoxical "high connectivity-low correlation" states.

Subsequently, eco-hydrological impacts were analyzed using hydrological, water quality, and plant physiological datasets. Results demonstrated robust positive correlations between hydrological connectivity and runoff magnitude. However, connectivity's influence on soil moisture exhibited spatiotemporal nonstationarity, attributed to bank irrigation interference and vadose zone transport lag effects. Hydrologically enhanced self-regulation capacity stabilized water quality fluctuations, while connectivity-driven riparian plant productivity displayed distance-decay relationships, transitioning from strong riverside correlations to weak upland linkages. Finally, leveraging ecological insights from "high connectivity-low correlation" regimes, we propose three-pronged management innovations: (1) deployment of

http://www.aloki.hu ● ISSN 1589 1623 (Print) ● ISSN 1785 0037 (Online)
DOI: http://dx.doi.org/10.15666/aeer/2304_71377151

isotope-integrated smart monitoring networks, (2) isotope-guided dynamic replenishment frameworks, and (3) connectivity-optimized riparian buffer designs.

The "graph theory-isotope tracing" coupled assessment framework developed here enables multidimensional connectivity quantification and effectively diagnoses engineered pseudo-connectivity (e.g., isotopic-hydraulic decoupling). This approach offers a paradigm for evaluating and managing urban rivers under intensified anthropogenic forcing.

Acknowledgements. The authors express the great gratitude to those who make careful inspection and give advice for the improvement of this paper. This study was financially supported by the General Project of Shenzhen University Stable Support Program (No.20200926182950001), the Shenzhen Polytechnic University Scientific Research Supporting Projects (No. 6022310035K), the Post-doctoral Later-Stage Foundation Project of Shenzhen Polytechnic University (No. 6020271006K), and the Guangdong Basic and Applied Basic Research Foundation (No. 2025A1515011110).

REFERENCES

[1] Alrehaili, A. M., Keller, C. K., Moore, B. C., Boll, J. (2024): Stable isotope hydrology of a polymictic lake: capturing transience of groundwater interactions. – Journal of Hydrology 639: 131551.
[2] Best, J. (2019): Anthropogenic stresses on the world's big rivers. – Nature Geoscience 12: 7-21.
[3] Bracken, L. J., Croke, J. (2007): The concept of hydrological connectivity and its contribution to understanding runoff-dominated geomorphic systems. – Hydrological Processes 21(13): 1749-1763.
[4] Cai, Y. J., Liang, J. S., Zhang, P. Y., Wang, Q. Y., Wu, Y., Ding, Y. R., Wang, H. J., Fu, C., Sun, J. J. (2021): Review on strategies of close-to-natural wetland restoration and a brief case plan for a typical wetland in northern China. – Chemosphere 285: 131534.
[5] Chen, S. Q., Rugenstein, J. K. C., Mulch, A. (2025): Stable isotope composition of surface waters across the Pamir, Central Asia: implications of precipitation seasonality. – Journal of Hydrology 653: 132815.
[6] Dang, L., Ma, C., Wang, H. X. (2025): Effects of vanishing power-law tails of river flows caused by damming on downstream hydrological connectivity. – Journal of Hydrology 646: 132317.
[7] Dansgaard, W. (1964): Stable isotopes in precipitation. – Tellus 4: 436-468.
[8] Fu, G. P., Zhao, L., Wu, J. F., Hu, Z. L., Hu, K., Dong, Y. (2020): Ecological function evaluation and restoration strategy of rivers in urban built-up areas: a case study of the Dasha River in Shenzhen. – Journal of Shenzhen University Science and Engineering 37(4): 372-380.
[9] Gao, Z. Q., Li, C. B., Zou, S. B., Xie, X. H., Wang, Y. F., Shen, N., Zhang, X. Y., Li, M. J. (2024): Riverine wetland dynamics and health assessment: a case study in the urban agglomerations along the Yellow River in China's Ningxia Hui Autonomous Region. – Ecological Indicators 162: 111965.
[10] Grill, G., Lehner, B., Thieme, M., Geenen, B., Tickner, D., Antonelli, F. (2019): Mapping the world's free-flowing rivers. – Nature 569(7755): 215-221.
[11] Guo, S. S., Li, L., Wang, S. L., Huang, J. C., Xie, X. T., Wang, Y. H. (2024): What are the dominant drivers and optimal thresholds for a healthy ecosystem in the Yellow River Basin, China? from a perspective of nonlinear nexus. – Ecological Indicators 162: 111997.

http://www.aloki.hu ● ISSN 1589 1623 (Print) ● ISSN 1785 0037 (Online)
DOI: http://dx.doi.org/10.15666/aeer/2304_71377151

[12] Han, Y. P., Xu, Y., Cao, R. X., Liu, Z. P. (2024): Optimization framework for eco-hydrological connectivity schemes based on graph theory and waterfront accessibility. – Journal of Hydrology: Regional Studies 56: 101975.
[13] Henderson, B. L., Bui, E. N., Moran, C. J., Simon, D. A. P. (2005): Australia-wide predictions of soil properties using decision trees. – Geoderma 124(3-4): 383-398.
[14] Hu, X. D., Deng, Y. W., Zhou, C., Shu, H. J., Wang, J., Wang, Z., Wang, Y. B., Zhao, J. S., Huang, W. Y., Xiao, H. B., Shi, Z. H. (2024): Chemodiversity of dissolved organic matter exports from subtropical humid catchment driven by hydrological connectivity. – Water Research 260: 121902.
[15] Jiang, X., Jiang, Z. Y., Li, Z. Y., Su, J., Tang, L. N., Wu, M. D., Wang, Y. J. (2025): A framework for the construction of effective landscape ecological network with integrating hydrological connectivity: a case study in Dongjiang River Basin, China. – Journal of Environmental Management 376: 124509.
[16] Kleine, K., Tetzlaff, D., Smith, A., Goldhammer, T., Soulsby, C. (2021): Using isotopes to understand landscape-scale connectivity in a groundwater-dominated, lowland catchment under drought conditions. – Hydrological Processes 35: e14197.
[17] Lei, M., Long, Y., Li, T. X., Ma, Y. C., Zhang, G. J., Peng, B., Li, Z. W., Liu, Y. J. (2024): Nitrogen dynamic transport processes shaped by watershed hydrological functional connectivity. – Journal of Hydrology 645: 132218.
[18] Li, B., Wan, R. R., Yang, G. S., Yang, S., Dong, L. F., Cui, J. L., Zhang, T. (2024): Centennial loss of lake wetlands in the Yangtze Plain, China: impacts of land use changes accompanied by hydrological connectivity loss. – Water Research 256: 121578.
[19] Liu, X., Xue, J., Chang, J. J., Sun, H. W., Zhao, Y., Li, F., Wang, S. K., Lei, Q. Y. (2025): Hydrological connectivity-mediated spatial vegetation patterns and regime shifts in drylands. – Ecological Indicators 171: 113194.
[20] Mu, J. X., Wu, Y., Qi, P., Chen, L. W., Yuan, Y. X., Wu, H. T. (2024): Spatial and temporal change of hydrological connectivity in the Wusuli River Basin. – Journal of Hydrology: Regional Studies 53: 101814.
[21] Qiao, K., Wang, W. X. (2024): The dual role of coastal mangroves: sinks and sources of microplastics in rapidly urbanizing areas. – Journal of Hazardous Materials 480: 136408.
[22] Shenzhen Water Authority. (2022): Shenzhen Water Resources Bulletin (2022). – Shenzhen Water Authority, Shenzhen.
[23] Shi, P., Zhou, D. M., Jiang, J., Ma, J., Zhu, X. Y., Zhang, J., Li, Z. H., Dong, Q. H. (2025): Ecosystem services value for water provisioning in the Shule River Basin of northwestern China: spatial and temporal evolution and drivers from 2000 to 2022. – Heliyon 11(2): e41907.
[24] Wan, D. J., Wang, J., Liu, X., Liu, Q. W., Chen, B. L., Chen, Y. H., Zhao, D. D., Liu, J. P. (2025): Identifying freshwater wetland suitable habitat through a hydrological-biological connectivity framework: a case study of Naoli River wetlands, China. – Ecological Indicators 170: 121993.
[25] Wang, Y. Q., Xian, C. F., Jiang, Y. Q., Pan, X. L., Ouang, Z. Y. (2020): Anthropogenic reactive nitrogen releases and gray water footprints in urban water pollution evaluation: the case of Shenzhen City, China. – Environment, Development and Sustainability 77(7): 6343-6361.
[26] Wang, Y. Q., Xue, H. J., Li, A. Q., Ma, X. F., Sun, A. L., Zhang, J. H. (2025): Spatial-temporal differentiation and influencing factors of ecosystem health in Three-River-Source national Park. – Ecological Indicators 171: 113183.
[27] Wu, J. N., Yang, B., Cheng, F., Zhao, F., Ma, S., Yuan, X., Zeng, H. H., Tang, C., Yang, K., Zhao, L. (2024): Decoding lake water dynamics to optimize watershed agriculture through isotopic analyses of memory effects and hydrological connectivity. – Ecological Indicators 169: 112826.
[28] Xu, G. L., Xu, Y. P., Wang, L. Y. (2012): Evaluation of river network connectivity based on hydraulic resistance and graph theory. – Advances in Water Science 23(6): 776-781.

http://www.aloki.hu ● ISSN 1589 1623 (Print) ● ISSN 1785 0037 (Online)
DOI: http://dx.doi.org/10.15666/aeer/2304_71377151

[29] Xue, F., Zhang, Q., Melack, J. M., Tang, H. W., Yuan, S. Y., Jia, Y. X., Xue, C. Y., Song, Y. Y. (2024): Floodplain lakes: linking hydrology to ecology and conservation. – Earth-Science Reviews 258: 104967.
[30] Yang, J. W., Huang, Y. L., Liu, X. P., Jing, R. Y., Liu, C. (2023): From collapse to the health of the aquatic ecosystem in Dasha River (2006–2021): a case study of Shenzhen city in the Guangdong-Hong Kong-Macao Greater Bay Area, China. – Environmental Science and Pollution Research 30: 49097-49107.
[31] Zarfl, C., Lumsdon, A. E., Berlekamp, J., Tydecks, L., Tockner, K. (2015): A global boom in hydropower dam construction. – Aquatic Sciences 77(1): 161-170.
[32] Zhang, J., Chen, H. S., Fu, Z. Y., Wang, F., Wang, K. L. (2023): Towards hydrological connectivity in the karst hillslope critical zone: insight from using water isotope signals. – Journal of Hydrology 617: 128926.
[33] Zheng, H. W., Tetzlaff, D., Birkel, C., Chmieleski, J., Comte, J. C., Freymueller, J., Goldhammer, T., Schmidt, A., Wohl, E., Soulsby, C. (2025): Hydrological connectivity and biogeochemical dynamics in the function and management of the lower Oder floodplain. – Journal of Hydrology 653: 132708.
[34] Zou, D. Y., Qi, Y. L., Gu, C. X., Hou, J. J., Pan, Y. P., Li, M. (2024): A comparison of microbial diversity, distribution patterns, and halogenated aromatics biodegrading genes in sediments of two urban rivers. – International Biodeterioration & Biodegradation 191: 105806.

http://www.aloki.hu ● ISSN 1589 1623 (Print) ● ISSN 1785 0037 (Online)
DOI: http://dx.doi.org/10.15666/aeer/2304_71377151